5-9-2017

Gödel's Universe

Kevin Roebuck

Gödel's Universe

Kevin Roebuck

Submitted in Partial Completion of the
Requirements for Commonwealth Honors in Physics

Bridgewater State University

May 9, 2017

Dr. Thomas Kling, Thesis Director
Dr. Ed Deveney, Committee Member
Dr. Jeff Williams, Committee Member

Gödel's Universe

Kevin Roebuck

Spring 2017

Contents

Abstract

In this thesis, a brief introduction of Albert Einstein's general theory of relativity is given. Included is a historical background of the theory and descriptions of spacetimes and cosmological models. From there, wave fronts of null geodesics in the Gödel metric emitted from point sources both at, and away from, the origin are examined to show the rotational and non-causal features of the Gödel spacetime. For constant time wave fronts emitted by sources away from the origin, we find blue sky metamorphoses where spatially disconnected portions of the wave front appear, connect to the main wave front, and then later break free and vanish. These blue sky metamorphoses in the constant time wave fronts highlight the non-causal properties of the Gödel metric. We also introduce a concept of physical distance along the null geodesics, in which the blue sky metamorphoses do not occur.

1 History of general relativity

The origins of general relativity, Albert Einstein's classical theory of gravity [Einstein (1916)], can be traced to the conceptual revolution that followed Einstein's introduction of special relativity in 1905. Newton's centuries-old gravitational force law describes the magnitude of attraction between two bodies of mass m_1 and m_2 as

$$F = \frac{Gm_1m_2}{r^2}, \tag{1}$$

where r is the distance between them and G is Newton's gravitational constant. Since the force on one mass depends on the position of the other mass at the same time, the force is an instantaneous interaction. This instantaneous signal is prohibited by special relativity, where no signal can travel faster than the speed of light. One might ask why anyone would switch from the wildly successful Newtonian view for this strange new relativistic view. One of the most compelling cases for relativity comes in the form of Maxwell's equations [Maxwell (1865)]. Maxwell's equations, together with the Lorentz force law, summarize the entire theoretical content of electrodynamics and are consistent with special relativity. As such, Newtonian gravity is, at best, an approximation to a more fundamental theory [Hartle (2003)].

Albert Einstein published his theory of gravitation, general relativity, in 1916. Einstein saw that the experimental fact that all bodies fall with the same acceleration in a gravitational field naturally led to an understanding of gravity in terms of the curvature of the union of space and time-spacetime. The theory explains gravity as a consequence of the curvature of spacetime, while in turn spacetime is a consequence of the presence of matter. To accurately describe the curvature of spacetime requires the use of differential geometry, in which scalars and vectors are expressed in terms of tensors. The equations

$$\left(R_{ab} - \frac{1}{2}Rg_{ab}\right) + \Lambda g_{ab} = 8\pi T_{ab} \tag{2}$$

are called the Einstein field equations, where R_{ab} is the Ricci curvature tensor, R is the Ricci curvature scalar, g_{ab} is the metric tensor, Λ is the cosmological constant, and T_{ab} is the energy-momentum tensor. The expression on the left describes the curvature of spacetime as determined by the metric, while the expression on the right describes the energy/matter content of spacetime [Hawking & Ellis(1973)].

2 What is a spacetime?

In everyday life, the space around us is often thought of in terms of flat, three-dimensional Euclidean space. In Euclidean space, every point is determined by three spatial coordinates, with the distance between two points given by the line element

$$ds^2 = dx^2 + dy^2 + dz^2. \tag{3}$$

A spacetime, then, is a system of coordinates that also includes a fourth, temporal coordinate. A given set of coordinates in this form is called an event. As known from differential geometry, the local neighborhood of points on a curved surface can be approximated by a plane. In a similar way, a curved spacetime can be locally approximated by a flat spacetime. The interval between two events of flat spacetime, better known as Minkowski space, may then be given locally as

$$ds^2 = -dt^2 + dx^2 + dy^2 + dz^2. \tag{4}$$

Note that the temporal and spatial coordinates differ in sign from each other and may be in the form (+, -, -, -) or (-, +, +, +). This form is necessary for the line element to be preserved under transitions between inertial frames (relative motion with constant velocity). These transitions are more commonly referred to as Lorentz transformations, and may be rotations or translations in four-space.

Though all curved spacetimes may be approximated as a plane locally, the spacetime of our universe is most certainly curved. This curvature may be expressed as

$$ds^2 = \sum_{a=0}^{\infty}\sum_{b=0}^{\infty} g_{ab}dx^a dx^b \equiv g_{ab}dx^a dx^b, \tag{5}$$

where x is the vector (t, x, y, z) and g_{ab} is the metric tensor. By assuming that the indices go over the values 0-3, we can remove the summation signs. The components of the metric tensor, which is needed to define distance along a curve when we are in non-cartesian coordinate systems, form a 4 x 4 matrix. As an example, the metric for Minkowski space is as follows:

$$g_{ab} = \begin{vmatrix} -1 & 0 & 0 & 0 \\ 0 & 1 & 0 & 0 \\ 0 & 0 & 1 & 0 \\ 0 & 0 & 0 & 1 \end{vmatrix}.$$

The metric determines particle motion, and Newton's Law of Gravity,

$$\nabla^2\phi = 4\pi G\rho, \tag{6}$$

where ϕ is the gravitational potential, G is the universal gravitational constant, and ρ is a continuous mass density, suggests that mass must fix the metric. Thus a tensor built from the metric and/or its derivatives that can substitute for $\nabla^2\phi$ in Newton's theory is needed. The metric tensor alone is not sufficient since coordinates can always be found such that the metric tensor becomes the Minkowski metric, which cannot simultaneously describe situations with and without mass. The first derivatives are not enough either as it can be shown

that coordinates can always be found in which the first derivatives are equal to zero. Thus, since the second derivatives cannot be shown to be zero with a clever choice of coordinates, it is clear that the tensor must include at least second derivatives of the metric [Alexander (2016)]. The result is the Ricci curvature tensor

$$R_{\alpha\beta} = \frac{\partial \Gamma^{\gamma}_{\alpha\beta}}{\partial x^{\gamma}} - \frac{\partial \Gamma^{\gamma}_{\alpha\gamma}}{\partial x^{\beta}} + \Gamma^{\gamma}_{\alpha\beta}\Gamma^{\delta}_{\gamma\delta} - \Gamma^{\gamma}_{\alpha\delta}\Gamma^{\delta}_{\beta\gamma}, \tag{7}$$

where the coefficients Γ^{k}_{ij} are the Christoffel symbols, which are constructed from the metric and its first derivatives

$$g_{\alpha\delta}\Gamma^{\delta}_{\beta\gamma} = \frac{1}{2}\left(\frac{\partial g_{\alpha\beta}}{\partial x^{\gamma}} + \frac{\partial g_{\alpha\gamma}}{\partial x^{\beta}} - \frac{\partial g_{\beta\gamma}}{\partial x^{\alpha}}\right). \tag{8}$$

If the metric is not diagonal, the matrix inverse of the metric has to be computed to solve the linear equation for the Γ's [Hartle (2003)].

3 Cosmological solutions

Because of the complexity of the field equations, one cannot find exact solutions except in spaces of rather high symmetry. Exact solutions are also idealized in that any region of spacetime is likely to contain many forms of matter, while one can obtain exact solutions only for rather simple matter content. Nevertheless, exact solutions give an idea of the qualitative features that can arise in GR, and so of possible properties of realistic solutions of the field equations [Stephani et al. (2003)].

A cosmological solution is a pseudo-Riemannian manifold with certain tensor fields that satisfies the Einstein field equations (Eq. 2). Any spacetime metric is a solution if no restriction is imposed on the energy-momentum tensor, since the field equations become just a definition of T_{ab}. Thus, assumptions about T_{ab} must be made, such as imposing symmetry conditions, like homogeneity (the curvature of any two points for a given time is the same) and isopetry (the universe looks the same in all directions), on the metric by restricting the algebraic structure of the Riemann tensor, adding field equations for the matter variables, or imposing initial and boundary conditions [Carroll (2001)]. Cosmological models typically show a universe to be approximately homogenous and isotropic on spatial distance scales above several hundred megaparsecs. Matter and radiation in galaxies, for example, are often approximated by smooth density distributions that are exactly uniform in space. As such, comsological models are designed to model what a given universe looks like on average.

4 Robertson-Walker metric

In cosmology, it is often assumed that our universe is, on a large enough scale, homogeneous and isotropic. From these assumptions, it can be shown that the

metric takes the form

$$ds^2 = -dt^2 + a^2(t)\left[\frac{dr^2}{1-kr^2} + r^2(d\theta^2 + sin^2(\theta)d\phi^2)\right], \tag{9}$$

the Robertson-Walker (RW) metric. Note that this metric is described using spherical coordinates in which the spatial position of a point is specified by a radial component, r, and polar angle, θ, and an azimuthal angle, ϕ. While the metric can be described using any coordinate system, it turns out to be more useful and natural to use spherical coordinates. The constant k is related to the curvature of space and can be -1, 0, or +1.

$$k = \begin{cases} -1, & \text{open universe;} \\ 0, & \text{flat universe;} \\ +1, & \text{closed universe.} \end{cases}$$

The $k = -1$ case describes an open universe, which is one with negative spatial curvature (described by hyperbolic space); $k = 0$ is a flat universe with no spatial curvature; and $k = +1$ is a closed universe with positive curvature analagous to the surface of a sphere. The function $a(t)$ is the scale factor, which describes the relative size of spatial surfaces. If $a(t)$ increases in time, the line element Eq. 9 describes an expanding universe, which is the case for the universe we live in. Also note that the above coordinates are comoving, meaning that a point which is at rest in the preferred frame of the universe has (r, θ, ϕ) constant.

The symmetry of the RW solutions requires that the energy-momentum tensor has the form of a perfect fluid whose density μ and pressure p are functions of the time coordinate only. This fluid can be thought of as a smoothed out approximation to the matter in the universe. The equation of conservation of energy takes the form

$$\mu = -\frac{3(\dot{\mu} + p)\dot{a}}{a}. \tag{10}$$

From this, it follows that the density decreases as the universe expands, and conversely that the density was higher in the past [Kurki-Suonio (2012)].

5 The Gödel metric

In 1949, Austrian mathematician Kurt Gödel introduced an exact solution of the Einstein field equations, in that there is homogeneity and isotropy about every point, that described a universe with rotational and non-causal features [Gödel(1949)]. In the Gödel universe, the spacetime rotates around every point, with increasing rotation as the distance from the observer increases. The study of Gödel's metric played an important historical role in understanding Mach's principle [Earman (1995)].

Though the Gödel universe is generally considered to be an unsuitable cosmological solution, it has a number of interresting properties that allow it to

serve as a test-bed for physics in other, more relevant and sometimes more complicated, spacetimes. The rotational properties, manifested in the metric by off-diagonal $dtd\phi$ terms, allow for closed time-like curves when the radius, r, is greater than $\log(1+\sqrt{2})$ [Hawking & Ellis(1973)]. An object following one of these curves would eventually end up at the exact moment in the past that it began the journey, implying that causality is not preserved. The existence of closed time-like curves makes this metric similar to the extreme Kerr (spin parameter $a^2 > m^2$) solution.

6 Equations of motion & boundary conditions

The Gödel spacetime metric is given by

$$ds^2 = dz^2 - \frac{2}{\omega^2}dt^2 + \frac{2}{\omega^2}dr^2 - \frac{2}{\omega^2}\left(\sinh^4 r - \sinh^2 r\right)d\phi^2 + \frac{4\sqrt{2}}{\omega^2}(\sinh^2 r)dt\,d\phi, \tag{11}$$

where ω is the vorticity of a pressure-free perfect fluid [Hawking & Ellis(1973)]. Due to the rotational symmetry of the metric, cylindrical coordinates are used here. In these coordinates, there is a closed null curve at $r_G = \log(1+\sqrt{2})$ and invariance under changes in z. To find the null geodesics, we consider the Lagrangian

$$\begin{aligned}\mathcal{L} &= \frac{1}{2}g_{ab}\dot{x}^a\dot{x}^b = 0 \\ &= \frac{1}{2}\dot{z}^2 - \frac{\dot{t}^2}{\omega^2} + \frac{\dot{r}^2}{\omega^2} - \frac{1}{\omega^2}\left(\sinh^4 r - \sinh^2 r\right)\dot{\phi}^2 + \frac{2\sqrt{2}}{\omega^2}(\sinh^2 r)\,\dot{t}\,\dot{\phi},\end{aligned} \tag{12}$$

where the dot denotes the derivative with respect to an affine parameter λ. From this, we have four Euler-Lagrange equations (t, r, ϕ, and z), of the form

$$\frac{\partial\mathcal{L}}{\partial q} = \frac{d}{d\lambda}\frac{\partial\mathcal{L}}{\partial\dot{q}} \tag{13}$$

which yield five 1st order ODEs and three constants of integration. The Euler-Lagrange equation for z is easily solved for $\dot{z}$, since momentum is conserved in the x direction:

$$\dot{z} = p_z. \tag{14}$$

The Euler-Lagrange equation for r becomes

$$\ddot{r} = \left(-2\sinh^3 r\cosh r + \sinh r\cosh r\right)\dot{\phi}^2 + 2\sqrt{2}(\sinh r\cosh r)\dot{t}\,\dot{\phi}. \tag{15}$$

The Euler-Lagrange equations for t and ϕ are more complicated. The $\dot{t}\dot{\phi}$ term means that the Euler-Lagrange equations for t and ϕ are coupled:

$$\frac{-2}{\omega^2}(\sinh^4 r - \sinh^2 r)\dot{\phi} + \frac{2\sqrt{2}}{\omega^2}(\sinh^2 r)\dot{t} = p_\phi \quad (16)$$

$$\frac{2\sqrt{2}}{\omega^2}(\sinh^2 r)\dot{\phi} - \frac{2}{\omega^2}\dot{t} = -p_t. \quad (17)$$

The negative sign in front of p_t allows positive time to be associated with generally increasing t values. After algebraically solving for $\dot{t}$ and $\dot{\phi}$ and introducing $v_r = \dot{r}$, we end up with five first order ordinary differential equations for light rays in the Gödel spacetime:

$$\dot{z} = p_z \quad (18)$$

$$\dot{r} = v_r \quad (19)$$

$$\dot{t} = \frac{\omega^2}{2}\left(\frac{\sqrt{2}\,p_\phi}{1+\sinh^2 r} + \frac{p_t(1-\sinh^2 r)}{1+\sinh^2 r}\right) \equiv f_t \quad (20)$$

$$\dot{\phi} = \frac{\omega^2}{2}\left(\frac{p_\phi}{\sinh^2 r\,(1+\sinh^2 r)} + \frac{\sqrt{2}\,p_t}{1+\sinh^2 r}\right) \equiv f_\phi \quad (21)$$

$$\dot{v}_r = \left(-2\sinh^3 r\cosh r + \sinh r\cosh r\right) f_\phi^2 + 2\sqrt{2}\sinh r\cosh r\, f_t f_\phi. \quad (22)$$

Wave fronts of null geodesics emitted from the origin at $r_o = 0$ as well as wave fronts for general points away from the origin but within the closed null curve at $r_G = \log(1+\sqrt{2})$ are examined. The condition that the geodesics are null geodesics is enforced by setting the Lagrangian to zero at $s = 0$, which we enforce by solving Eq. 12 for v_r at the initial point. This leads to

$$v_{ro} = \pm\sqrt{f_{to}^2 - \frac{\omega^2}{2}p_z^2 + (\sinh^4 r_o - \sinh^2 r_o)f_{\phi o}^2 - 2\sqrt{2}(\sinh^2 r_o)f_{\phi o}f_{to}} \quad (23)$$

where r_o is the initial radius and f_{to} and $f_{\phi o}$ are the functions defined in Eqs. 20 and 22 evaluated at the initial radius. By requiring the term under the square root to be greater than or equal to zero, limits will be set on the initial momentum p_z and p_ϕ.

For null geodesics at, or passing through, the origin, the angular momentum p_ϕ must be zero so that the $\sinh^2 r$ term in the denominator of f_ϕ in Eq. 22 does not lead to an infinity. The initial conditions for null geodesics beginning at the origin consist of $r_o = 0$, $t_o = 0$, and $z_o = 0$, where Eq. 23 is then

$$v_{ro} = +\frac{\omega}{2}\sqrt{\omega^2 p_t^2 - 2p_z^2}. \quad (24)$$

From this, the range of the z momentum, $-\sqrt{\omega^2 p_t^2/2} < P_z < +\sqrt{\omega^2 p_t^2/2}$, is implied. The time momentum, p_t, is free to take any value, so we can choose p_t=1 and ω=1. At the origin, the initial value of ϕ is free, and different choices

of ϕ_o in the range $0 < \phi_o < 2\pi$ result in a circle's worth of different null geodesics spanning the $z = 0$ plane.

Null geodesics beginning at $r_o \neq 0$ have different initial conditions and limitations on the momenta. The null geodesic condition is first enforce by setting v_{ro} as in Eq 23. To ensure v_{ro} is real, the z momentum is restricted to

$$|p_z| < \sqrt{\frac{2}{\omega^2}\left(f_{to}^2 + (\sinh^4 r_o - \sinh^2 r_o) f_{\phi p}^2 - 2\sqrt{2}\sinh^2 r_o f_{to} f_{\phi o}\right)}. \tag{25}$$

Requiring the radicand in Eq. 25 to be positive yields the range of momentum p_ϕ.

$$p_{\phi\pm} = p_t \sinh^2 r_o \left(\sqrt{2} \pm \sqrt{2 + \frac{1 - \sinh^2 r_o}{\sinh^2 r_o}}\right). \tag{26}$$

Since there are no restrictions on p_t, we generally set$p_t = 1$ to ensure that time increases. Choosing an initial p_ϕ within the limits defined by Eq. 26 and thus a value of p_z in the range given by Eq. 25 results in a sphere's worth of null geodesics originating at a point $(t_o = 0, r_o \neq 0, \phi_o = 0, z_o = 0)$. Equation 23 then sets v_{ro} for initially incoming and outgoing null rays.

7 Numerical Integration

In order to integrate the null geodesics, a modification of the Runge-Kutta-Fehlberg 4-5 adaptive step-size approach is implemented. The classical fourth-order Runge-Kutta formula is given by

$$\begin{aligned}
k_1 &= hf(x_n, y_n) \\
k_2 &= hf(x_n + \frac{h}{2}, y_n + \frac{k_1}{2}) \\
k_3 &= hf(x_n + \frac{h}{2}, y_n + \frac{k_2}{2}) \\
k_4 &= hf(x_n + h, y_n + k_3) \\
y_{n+1} &= y_n + \frac{k_1}{6} + \frac{k_2}{3} + \frac{k_3}{3} + \frac{k_4}{6} + O(h^5),
\end{aligned} \tag{27}$$

which advances a solution from x_n to $x_{n+1} \equiv \mathrm{x}_{n+h}$, where h is the step size. For a set of n differential equations, the values of the independent variables are inputted, which yield new values which are stepped by a stepsize h (which can be positive or negative). To calculate the right-hand side, function derivatives and values of the derivatives at the starting point are needed. Also of note is that the Runge-Kutta method treats every step in a sequence of steps in identical manner. Prior behavior of a solution is not used in its propagation, since any

point along the trajectory of an ordinary differential equation can serve as an initial point [Press (1992)].

All of the code for this research was written in C++. The snippet of code in Fig. 1 is an example of a fourth order Runge-Kutta method before the adaptive step size was implemented. The ray handler, which sets the initial conditions of each individual light ray in a given wave front, is shown in Fig. 2.

```
void GodelRay::dump(std::ostringstream &stream) {
    double x = r * cos(phi);
    double y = r * sin(phi);
    stream << "Id: " << getElementId() << " Pz:" << Pz << " Pt:" << Pt <<  " t: " << t <<
            " , x: " << x << " , y: " << y << " , z: " << z << " , r: " << r << " , phi:" << phi <<
            " , vr: " << vr << " , ell: " << ell << " , lambda: " << lambda << std::endl;
}

void GodelRay::computeRay() {
    double k1phi = h * fphi(Pphi, Pt, w, r);
    double k1t   = h * ft(Pphi, Pt, w, r);
    double k1vr  = h * vr_dot(Pphi, Pt, w, r);
    double k1r   = h * vr;
    double k1ell = h * elldot(Pphi, Pt, w, r, Pz, vr);

    double k2phi = h * fphi(Pphi, Pt, w, r + k1r/2.0);
    double k2t   = h * ft(Pphi, Pt, w, r + k1r/2.0);
    double k2vr  = h * vr_dot(Pphi, Pt, w, r + k1r/2.0);
    double k2r   = h * (vr + k1vr/2.0);
    double k2ell = h * elldot(Pphi, Pt, w, r + k1r/2.0, Pz, vr + k1vr/2.0);

    double k3phi = h * fphi(Pphi, Pt, w, r + k2r/2.0);
    double k3t   = h * ft(Pphi, Pt, w, r + k2r/2.0);
    double k3vr  = h * vr_dot(Pphi, Pt, w, r + k2r/2.0);
    double k3r   = h * (vr + k2vr/2.0);
    double k3ell = h * elldot(Pphi, Pt, w, r + k2r/2.0, Pz, vr + k2vr/2.0);

    double k4phi = h * fphi(Pphi, Pt, w, r + k3r);
    double k4t   = h * ft(Pphi, Pt, w, r + k3r);
    double k4vr  = h * vr_dot(Pphi, Pt, w, r + k3r);
    double k4r   = h * (vr + k3vr);
    double k4ell = h * elldot(Pphi, Pt, w, r + k3r, Pz, vr + k3vr);

    double x = r * cos(phi);
    double y = r * sin(phi);
    double dist = sqrt((x-0.5) * (x-0.5) + y*y);

    phi    = phi + k1phi/6.0 + k2phi/3.0 + k3phi/3.0 + k4phi/6.0;
    t      = t   + k1t/6.0   + k2t/3.0   + k3t/3.0   + k4t/6.0;
    vr     = vr  + k1vr/6.0  + k2vr/3.0  + k3vr/3.0  + k4vr/6.0;
    r      = r   + k1r/6.0   + k2r/3.0   + k3r/3.0   + k4r/6.0;
    ell    = ell + k1ell/6.0 + k2ell/3.0 + k3ell/3.0 + k4ell/6.0;
    z      = z   + h * Pz;
    lambda = lambda + h;
```

Figure 1: An example of the coded Runge-Kutta method. Based on our equations of motion, this steps the rays forward producing new values for the various parameters. After numerous iterations, the values for the ray at each step are calculated.

```
void GodelRayHandler::init() {
    int numRaysDim1 = (int)getArgument("nrays1");
    int numRaysDim2 = (int)getArgument("nrays2");
    double stepsize = getArgument("stepsize");

    for(int i=1; i<numRaysDim1; i++) {
        for (int j = 1; j < numRaysDim2; j++) {

            double w          = 1.0;
            double r          = 0.5;

            double Pt           = getArgument("Pt");
            double Pphilim1_val = Pphi_lim1(Pt, r);
            double Pphilim2_val = Pphi_lim2(Pt, r);
            double Pphi         = Pphilim2_val +((double)i) *(Pphilim1_val-Pphilim2_val)/numRaysDim1;
            double Pz           = -GodelRay::func_Pz(Pphi, Pt, w, r) + ((double)j)/numRaysDim2*2*GodelRay::func_Pz(Pphi, Pt,w,r);
            double vr           = GodelRay::func_vr(Pphi, Pt, w, r, Pz);

            addElement(new GodelRay(w, r, Pphi, Pt, Pz, vr, stepsize));
            addElement(new GodelRay(w, r, Pphi, Pt, Pz, -vr, stepsize));
        }
    }
}

void GodelRayHandler::setParameters() {
    addParameter("nrays1", 16);
    addParameter("nrays2", 4);
    addParameter("Pt", -1.414213462);
    addParameter("stepsize", 0.01);
}
```

Figure 2: A portion of the ray handler from the code. The handler's function is to generate the points that will later be plotted for visualization.

8 Wave Fronts of Constant Time

Null wave fronts of constant coordinate time in the Gödel spacetime created by point sources both at, and away from, the origin are explored. Wave fronts originating at points away from the origin are heavily impacted by the non-causal features of the metric.

We begin by considering the wave front in the $z = 0$ plane emitted from a point source at the origin. The wave front is the surface of constant t given $r_o = 0$, $p_z = 0$, and $p_\phi = 0$ while varying ϕ_o in the range zero to 2π. At any given time, the wave front itself is circular. Figure 3 shows that the wave front expands from the origin to the radius r_G and rebounds, closing back up to a point before expanding out again. The local directions of null geodesics in these expanding wave fronts, shown in Fig. 4, help display the rotational aspects of the Gödel spacetime. Because r_G is a null curve, the wave front rotates faster as it gets closer to r_G.

Six plots at successive times of constant coordinate time wave fronts emitted from a point source at the origin are shown in Fig. 5. The wave front begins as a sphere and, since the rays that travel more radially, with lower p_z values, reach the radius r_G first, they rebound earlier than rays travelling more along the axis of the cylinder. Each individual ray travels in a helical motion as in Fig. 6. Since these rays all pass repeatedly through points on the z axis, the circle's worth of points with the same p_z value and differing initial ϕ values collapse simultaneously along the z axis. There are always at most two twist points, and the wave front cycles in visual appearance between the second and final pictures.

Towards the end of the wave front, we see a cusp ridge. Cusp ridges are stable features of wave front singularities in the sense that small perturbations of the system do not remove them [Arnol'd(1992)]. This form of wave front singularity is common in wave fronts with axial symmetry. The cusp ridges appear when a circular portion of the wave front with the same p_z value, but different intial ϕ values catches up with and passes a different circle with a slightly larger p_z value.

Next, we consider wave fronts emitted by a point source away from the origin in the $z = 0$ plane. These wave fronts will still be from the viewpoint of an observer standing at the origin. Figure 7 shows the advancement of the coordinate time, t, as a function of the radial coordinate, r, for a null geodesic with initial conditions $r_0 = 0.5$, $\phi_0 = t_0 = z_0 = 0$, $p_t = +1$, $p_\phi = 0.35$, and $p_z = 0$. In terms of the affine parameter, both the t and r coordinates advance smoothly in s, but the time coordinate undergoes a brief period where it decreases with the affine parameter, leading to the loop in Fig. 7. As a result, the null geodesic exits the observable region $r < r_G$ at time t_A and re-enters at an earlier time t_B.

Figure 8 shows a constant time wave front emitted from $r_0 = 0.5$, in the $z = 0$ plane. To achieve an sphere's worth of initial directions, p_ϕ is varied and v_{r0} is allowed to take on positive and negative values. As with the wave fronts emitted at the origin, we use $x = rcos\phi$ and $y = rsin\phi$ to plot the spatial positions, even though we ultimately consider the wave front outside $r = r_G$ to be un-observable. This choice does, however, allow us to highlight the fact that a blue sky metamorphoses occurs outside the observable region. This portion of the wave front re-enters the observable region and connects to the portion of the wave front that proceeded uniformly from the point source.

Because these wave fronts are not expanding from the origin, the axial symmetry is broken and new wave front singularities arise. We see the appearance of a portion of the wave front "out of thin air" or "out of the blue sky." This segment of the wave front has a "sickle" shape [Arnol'd(1992)]. These sickles connect to the main portion of the wave front and two cusp singularities appear, although only one is inside the observable region. Following the wave front in time, a new set of sickles breaks free from the main wave front and vanishes, again outside the observable region.

Figure 9 shows the appearance of a portion of the constant time wave front that has entered the observable region due to the blue sky metamorphosis. This initially disconnected portion of the wave front merges with the outward expanding wave front slightly later. In Fig. 8, we see two views of the wave front at the same time from the top and bottom. We once again see the formation of cusp ridges towards both ends of the wave front. Unlike with the $r_0 = 0$ case however, the twist points and circular cusp ridges are no longer symmetric with a line parallel to the z axis. Each circular cusp ridge tilts relative to the $x - y$ plane. In addition, there is a new cusp ridge along the bottom where the sickles from the blue sky metamorphosis have joined the overall wave front.

9 Wave Fronts of Constant Distance

The Gödel metric is given by

$$ds^2 = dz^2 - Adt^2 + \frac{2}{\omega^2}dr^2 - Cd\phi^2 + Bdtd\phi, \tag{28}$$

Inside the observable region, $r < r_G$, we will introduce a time-like coordinate τ related to t and ϕ by

$$d\tau = \sqrt{A}dt - \frac{B}{2\sqrt{A}}d\phi. \tag{29}$$

In terms of this new coordinate, we see that the metric becomes diagonal and there is no mixing of the τ and ϕ coordinates:

$$ds^2 = -d\tau^2 + \frac{2}{\omega^2}dr^2 + dz^2 + \left(\frac{B^2}{4A} - C\right)d\phi^2. \tag{30}$$

The function in front of $d\phi^2$,

$$\frac{B^2}{4A} - C = \frac{2}{\omega^2}(\sinh^4 r + \sinh^2 r),$$

is manifestly positive, so under this coordinate transformation, we can define a physical distance δ_p along the light ray by integrating

$$\delta_p = \int_i^f ds \sqrt{\frac{2}{\omega^2}\dot{r}^2 + \dot{z}^2 + \frac{2}{\omega^2}(\sinh^4 r + \sinh^2 r)\dot{\phi}^2} \tag{31}$$

for $r < r_G$.

Outside the observable region, we introduce a coordinate Φ defined by

$$d\Phi = \sqrt{C}d\phi - \frac{B}{2\sqrt{C}}dt. \tag{32}$$

In terms of this coordinate, the metric takes the form

$$ds^2 = -d\Phi^2 + \left(\frac{B^2}{4C} - A\right)dt^2 + \frac{2}{\omega^2}dr^2 + dz^2 \tag{33}$$

and the term in front of dt^2,

$$\frac{B^2}{4C} - A = \frac{2}{\omega^2}\left(\frac{2\sinh^2 r}{\sinh^2 r - 1} - 1\right),$$

is positive for $r > r_G = \log(1 + \sqrt{2})$. In these coordinates, $d\Phi$ measures a time interval and the spatial 3-metric is identified by the remaining three terms. Thus for $r > r_G$, the physical distance is integrated from

$$\delta_p = \int_i^f ds \sqrt{\frac{2}{\omega^2}\dot{r}^2 + \dot{z}^2 + \frac{2}{\omega^2}\left(\frac{2\sinh^2 r}{\sinh^2 r - 1} - 1\right)\dot{t}^2}. \tag{34}$$

In practice, we are integrating the null geodesics, Eqs. 18-22 numerically. To keep track of the physical distance along the null geodesics, we simultaneously integrate a sixth ordinary differential equation

$$\dot{\delta}_p = \begin{cases} \sqrt{\frac{2}{\omega^2} v_r^2 + p_z^2 + \frac{2}{\omega^2}(\sinh^4 r + \sinh^2 r) f_\phi^2} & r < r_G \\ \sqrt{\frac{2}{\omega^2} v_r^2 + p_z^2 + \frac{2}{\omega^2}\left(\frac{2\sinh^2 r}{\sinh^2 -1} - 1\right) f_t^2} & r > r_G \end{cases} , \tag{35}$$

where we have used the form of the differential equations. We will use the boundary condition $\delta_p = 0$ at $s = 0$. By construction, the physical distance δ_p will be a monotonically increasing function along the null geodesics, regardless of the origin of the wave fronts. At the boundary $r = r_G$, the physical distance δ_p is continuous with a discontinuity in the first derivative.

Three successive constant δ_p wave fronts are shown in Fig. 10 for a null wave front emitted from the origin. We see that the overall shape of the constant $delta_p$ wave fronts are similar to those of constant t, except that the cusp ridges have vanished. Rings with the same p_z values remain stacked and do not pass each other as they do in the constant time case. The constant δ_p wave fronts rotate in the same manner as the constant t wave fronts.

Three successive wave fronts of constant δ_p for wave fronts emitted from $r_0 = 0.5$ are shown in Fig. 11. The light rays that make up the wave front continue to leave and re-enter the $r < r_G$ observable region, and so in the central panel of this figure, we do see a disconnected portion of the wave front re-entering the observable region, but we do not see any blue sky metamorphoses. There is simply a portion of the wave front that has exited the observable region and is re-entering after traveling some physical distance. Also note that the cusp ridges present in the constant time wave fronts have disappeared.

10 Discussion

Wave fronts of null geodesics in the Gödel spacetime emitted both at, and away from, the origin are examined. The non-causal features of the spacetime manifest themselves for wave fronts emanating from a point at $r_0 \neq 0$ since null geodesics extend outside the radius $r = r_G$ and the time coordinate along these geodesics is not progressing at a constant rate. In this case, a blue sky metamorphosis are developed where a portion of the wave front appears spatially disconnected from the main wave front.

Wave fronts of constant physical distance provide further insight into the evolution of wave fronts in the Gödel universe. The cusp ridges present in the constant time wave fronts vanish here. The removal of what is generally considered to be a stable feature under small system perturbations is interesting and is a potential topic of further investigation.

Though these properties are interesting in their own right, the main reason we are looking at the Gödel metric is to learn about the similar Kerr metric.

Both metrics have off-diagonal terms associated with rotational features. Another similarity is with the extreme Kerr (spin parameter $a^2 > m^2$) solutions, wherein closed time-like curves are allowed. Thus, the work done on the Gödel universe regarding the idea of constant physical distance will be applied directly to the Kerr metric.

Acknowledgements

The author extends a special thanks to his mentor Dr. Thomas Kling for his guidance in physics and in life in general. The author also thanks Eric Grotzke for developing the software platform that produced most of the visualizations presented in this thesis.

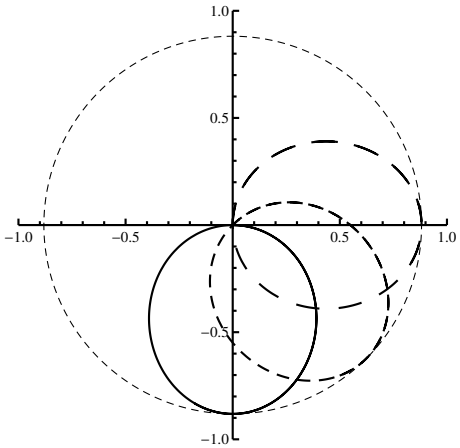

Figure 3: Three null geodesics with $p_z = 0$ originating at $r_0 = 0$. The solid, short dashed, and long dashed geodesics correspond to initial ϕ values 0, $\pi/4$, and $\pi/2$. Each null geodesic's path forms a closed loop extending out to the lightly dashed circle of radius r_G=log$(1 + \sqrt{2})$.

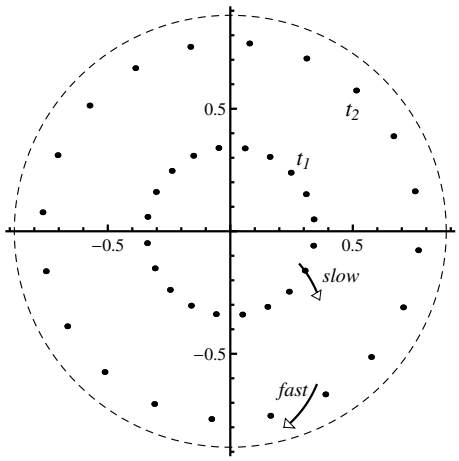

Figure 4: Dots outline two null geodesic wave fronts of constant coordinate time emitted by a point source at the origin for $p_z = 0$. The inner wave front is at a time t_1, with the outer wave front at a later time t_2. The solid curves show the local directions of the null geodesics. The front expands outwards with increasing rotation as the distance from the source increases.

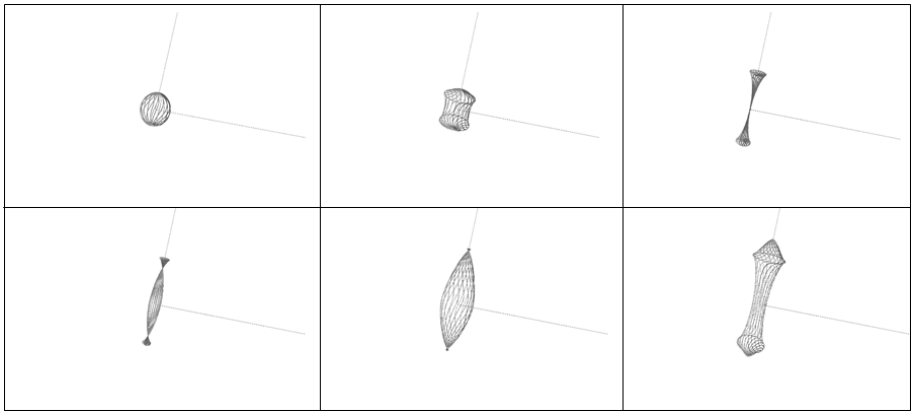

Figure 5: Null wave fronts of constant coordinate time emitted from a point source at the origin. The z axis points towards the upper right corner, and the viewpoint is fixed in all frames. An initial spherical front develops a set of cusp ridges as the wave front stretches vertically and oscillates radially. The wave front cycles between the second and sixth frame as time advances.

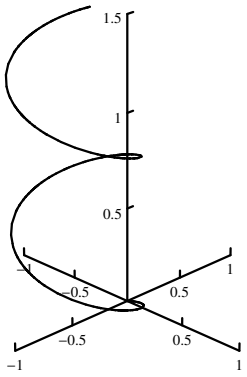

Figure 6: A null geodesic with $p_z = 0.125$ and initial $\phi_0 = 0$. The positive y axis points towards the upper right. The null geodesic is an ellipse in the x-y plane and spirals upwards in the positive z-direction.

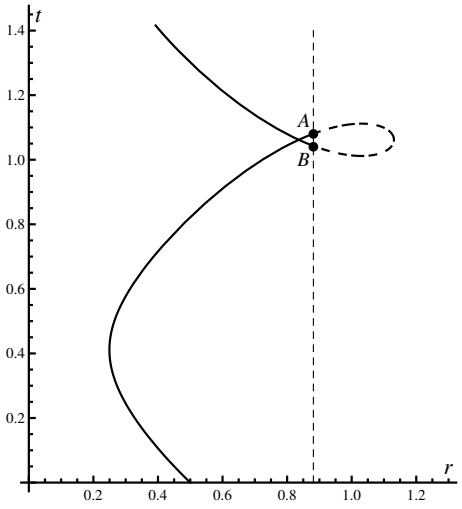

Figure 7: Plot of coordinate time vs. the radial component for a null geodesic with $p_z = 0$ and initial $p_\phi = 0.35$ originating at $r_0 = 0.5$. The dotted line shows the radius r_G=log$(1+\sqrt{2})$. Upon crossing this radius, the time coordinate loops back such that the time of re-entry, t_B, is less than the time of exit, t_A.

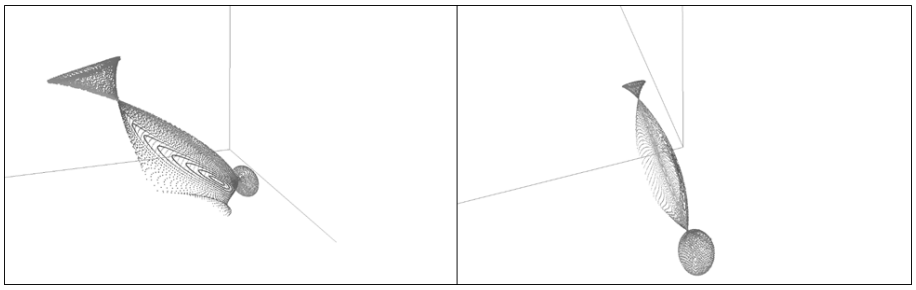

Figure 8: A top and bottom view at the same time of a wave front of light emitted from a position $r_0 = 0.5$ at a late time. A cusp ridge forms along the bottom side of the wave front where the lips of the blue sky metamorphosis have attached. The top view shows a cusp ridge on each end of the wave front

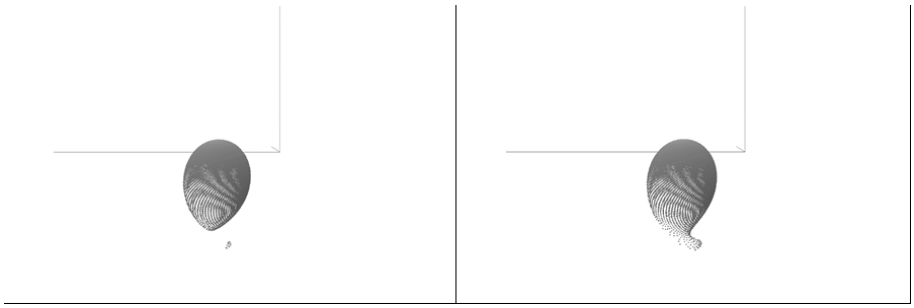

Figure 9: On the left, a portion of the wave front created in a blue sky metamorphosis appears along the cylinder of radius r_G centered at the origin and then combines with the main wave front,as shown at a later time on the right. The positive z axis points into page.

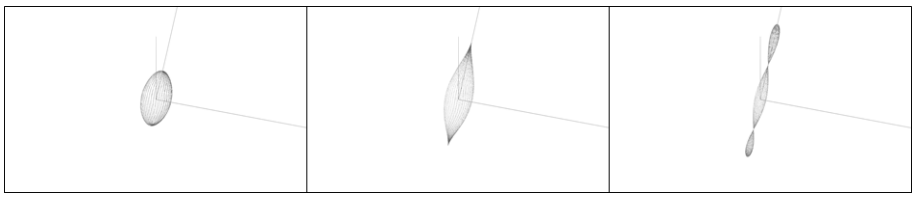

Figure 10: Wave fronts of constant physical distance in the Gödel space time emitted from the origin. The z axis is oriented up and towards the right to best show the features of the wave front. The cusp ridge present in the constant time wave fronts is missing in the wave fronts of constant physical distance.

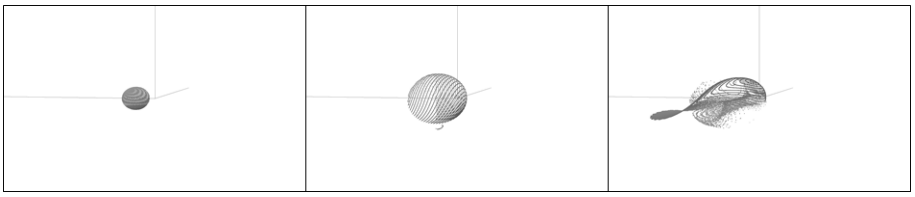

Figure 11: Wave fronts of constant physical distance emitted from $r_0 = 0.5$. The cusp ridge vanishes compared to the wave fronts of constant time. Portions of the wave front continue to re-enter from outside the observable region $r < r_G$, but no longer demonstrate the blue sky metamorphosis. The z axis is oriented slightly into the page to best show the detached incoming portion of the constant distance wave front.

References

[Einstein (1916)] A. Einstein, *The Foundation of the General Theory of Relativity*, Ann. der Physik 49, 769, (1916)

[Maxwell (1865)] J. Maxwell, *A dynamical theory of the electromagnetic field*, Philosophical Transactions of the Royal Society of London. 155: 459–512., (1865)

[Hartle (2003)] J. Hartle, *Gravity: An Introduction to Einstein's General Relativity*, Addison-Wesley, (2003)

[Hawking & Ellis(1973)] S. Hawking & G.F.R. Ellis, *The Large Scale Structure of Space-time*, Cambridge University Press (1973)

[Alexander (2016)] G. Alexander, `http://www2.warwick.ac.uk/fac/sci/physics/current/teach/module_home/px436/notes/lecture12.pdf`, (2016)

[Stephani et al. (2003)] H. Stephani, `http://catdir.loc.gov/catdir/samples/cam033/2002071495.pdf`, (2003)

[Carroll (2001)] S. Carroll, `https://preposterousuniverse.com/wp-content/uploads/2015/08/grtinypdf.pdf`, (2001)

[Kurki-Suonio (2012)] H. Kurki-Suonio, `http://www.helsinki.fi/~hkurkisu/cosmology/Cosmo3.pdf`, (2012)

[Gödel(1949)] K. Gödel, Rev. Mod. Phys. **21**, 447-450 (1949)

[Earman (1995)] J. Earman, *Bangs, Crunches, Whimpers and Shrieks: Singularities and Acausality in Relativitistic Spacetimes*, Oxford Univ. Press (1995)

[Press (1992)] Press, William H. and Teukolsky, Saul A. and Vetterling, William T. and Flannery, Brian P., *Numerical Recipes in C (2Nd Ed.): The Art of Scientific Computing*, Cambridge University Press (1992)

[Arnol'd(1992)] V.I. Arnol'd, *Catastrophe Theory*, Springer-Verlag (1992)